Available online at www.sciencedirect.com
ScienceDirect
International Journal of Multiphase Flow 33 (2007) 1205–1221
International Journal of Multiphase Flow
www.elsevier.com/locate/ijmulflow

# Experimental investigation of three-phase flow in a vertical pipe: Local characteristics of the gas phase for gas-lift conditions

M.N. Descamps [a], R.V.A. Oliemans [a,*], G. Ooms [b], R.F. Mudde [a]

[a] J.M. Burgerscentrum for Fluid Mechanics, Delft University of Technology, Multi-Scale Physics, Prins Bernhardlann 6, 2628 BW Delft, The Netherlands

[b] J.M. Burgerscentrum for Fluid Mechanics, Delft University of Technology, Laboratory for Aero- and Hydrodynamics, Mekelweg 2, 2628 CD Delft, The Netherlands

Received 26 September 2006; received in revised form 25 May 2007

**Abstract**

Laboratory experiments have been performed on the flow of oil, water and air through a vertical pipe in order to study the gas-lift technique for oil–water flows. Special attention was paid to the phase inversion phenomenon, by which the continuous phase switches to the dispersed phase and vice versa. By using different types of gas injectors the influence of the bubble size of the injected air on the efficiency of the gas-lift technique (in particular at the point of phase inversion) was studied. Also the gas and liquid mixture velocities were varied. The air bubbles were detected by means of optical fibre probes. Local measurements of the time-averaged gas volume fraction, bubble size and bubble velocity were carried out, as well as pressure measurements.

Phase inversion is associated with a sharp increase of the pressure gradient. With air injection the pressure gradient (for the oil–water–air flow) is always significantly smaller than for the case of oil–water flow, except at the point of phase inversion where the pressure drop can be even be higher than for oil–water flow. It was also found that air injection does not significantly change the critical concentration of oil and water where phase inversion occurs. An important phenomenon to explain these results is, that the presence of the dispersed (oil or water) phase has a significant influence on the bubble size. Also the influence of the gas flow rate on the distribution of the oil and water phases in a cross-section of the pipe plays a significant role.


*Keywords:* Gas-lift; Phase inversion; Bubbles; Oil–water flow

## 1. Introduction

In the oil industry oil–water flows often occur. Many studies have been carried out to understand and predict the phenomenon of phase inversion in such flows, whereby the continuous phase (oil or water) becomes

* Corresponding author. Tel.: +31 15 27 81323; fax: +31 15 278 2838.
*E-mail address:* R.V.A.Oliemans@TUDelft.nl (R.V.A. Oliemans).

0301-9322/$ - see front matter © 2007 Elsevier Ltd. All rights reserved.
doi:10.1016/j.ijmultiphaseflow.2007.06.001

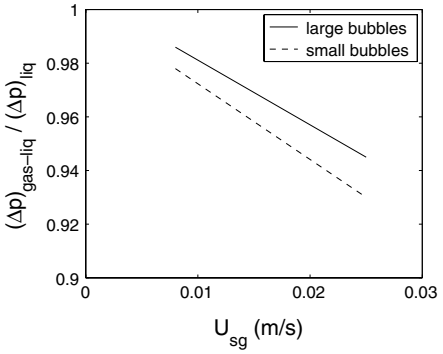


Fig. 1. Air–water pressure drop normalized by the water pressure drop, for vertical pipe flow (after Guet, 2004).

the dispersed phase and vice versa (Brauner and Ullmann, 2002; Chesters and Issa, 2004; Ioannou et al., 2005; Piela et al., 2006). However, not much research has been done concerning the effect of gas injection on inversion in an oil–water flow. This situation is, for instance, relevant for the gas-lift technique. In this technique gas is injected at the bottom of a production pipe (through which oil and water are flowing) in order to reduce the gravitational pressure drop in the well. This results in an increase of the oil flow rate in the pipe.

In practice gas is injected from valves attached to the pipe wall, which generates large bubbles. Previous work (Guet et al., 2003) with water and air indicated that the gas-lift efficiency can be improved by injecting small bubbles. The gravitational pressure drop is then reduced because: (i) the rise velocity of small bubbles is lower, and hence the residence time and void fraction in the pipe are higher, (ii) small bubbles are more evenly distributed over the cross-section of the pipe, which increases the gas void fraction, (iii) small bubbles postpone the transition from bubbly flow to slug flow, which is an undesirable operating condition for gas-lift. The effect of small bubbles on the reduction of the pressure gradient can be seen for the case of air–water flow on Fig. 1.

For the case of an oil–water flow the phase inversion phenomenon can have a significant effect on the efficiency of the gas-lift technique. At the point of phase inversion oil and water form a very viscous mixture leading to a high friction with the pipe wall and thus to a high pressure gradient (Brauner, 1998). In terms of oil production this condition is undesirable. Therefore, in our previous study (Descamps et al., 2006) three-phase (oil–water–air) flow experiments have been carried to investigate the influence of gas injection on oil–water phase inversion in a vertical pipe. Regarding the influence of gas injection it was shown that: (i) it does not change the water fraction at which phase inversion occurs, (ii) it increases the pressure gradient at phase inversion and (iii) the pressure gradient at phase inversion becomes higher when the bubble size is reduced, which contradicts previous work on air–water flow (Guet et al., 2003). To explore these results in more detail additional experiments concerning the influence of air injection on oil–water phase inversion in a vertical pipe were carried out with new instrumentation. In Section 2 the experimental set-up and the measurement techniques are described. Some preliminary measurements for an oil–water flow are presented in Section 3 in order to characterize the phase inversion process. In Section 4 the influence of gas injection on an oil–water flow is described for two different injectors (and hence different bubble sizes). In Section 5 the influence of the liquid and gas flow rates is reported for one of the gas injectors. Finally, conclusions are drawn is Section 6.

## 2. Experimental set-up

The first set of experiments (reported earlier in Descamps et al., 2006) was performed at the Shell Donau Loop facility, Rijswijk, The Netherlands. For the present work a new experimental set-up has been specially designed and built at the Kramers Laboratorium, Delft University of Technology, The Netherlands. The details of the two facilities are given in Table 1. The major differences concern the use of tap water instead of salted water, which will influence the bubble size, and the lower oil viscosity. Also there may be some variations due to the fact that in the present set-up gas is separated at the top (the pressure is atmospheric at the top of the pipe) whereas in the previous study the gas was separated at the bottom of the pipe.

Table 1
Physical properties of liquids used

| | Kramers lab | Shell |
|---|---|---|
| Pipe dimensions | 50 mm * 7 m | 82.8 mm * 15 m |
| Pipe material | Perspex and PVC | Steel |
| Maximum liquid velocity | 1.8 m/s | 6 m/s |
| Separation | Gas separated at the top | Three-phase in-line separation |
| Separator volume | 0.2 $m^3$ | 20 $m^3$ |
| Gas injection | Nozzle and ring injector | Nozzle and ring injector |
| *Fluids properties* | | |
| Water | Tap water<br>$\rho = 1000$ kg/$m^3$<br>$\mu = 1$ mPa s<br>$\sigma_{water/air} = 72.8$ mN/m | Brine<br>$\rho = 1060$ kg/$m^3$<br>$\mu = 0.85$ mPa s<br>$\sigma_{water/air} = 50.7$ mN/m |
| Oil | Shell Macron<br>$\rho = 794$ kg/$m^3$<br>$\mu = 3.1$ mPa s<br>$\sigma_{oil/air} = 24.20$ mN/m | Vitrea 10<br>$\rho = 830$ kg/$m^3$<br>$\mu = 7.5$ mPa s<br>$\sigma_{oil/air} = 30.3$ mN/m |
| Interfacial tension | $\sigma_{water/oil} = 21.8$ mN/m | $\sigma_{water/oil} = 20.2$ mN/m |

## 2.1. Description of the set-up

The loop is approximately 7 m high with an internal pipe diameter of 50 mm, and is operated in the turbulent flow regime. The pipes are made out of transparent perspex and PVC. Air is injected from the bottom and separated at the top via a gas–liquid separator (Fig. 2). Two types of gas injector are used: the porous ring injector, creating small bubbles, and the nozzle injector, creating larger bubbles. An example of the different gas fraction distribution obtained by changing the injector is shown later (Fig. 7). The liquid flow rate can be created by gas injection only (natural convection) or by a centrifugal pump (forced convection).

There is no in-line separation of oil and water, so the loop is filled with oil and water at the desired concentration before the start of the measurements. The separator is only used at the end of an experiment. For the Reynolds number considered here ($Re > 10{,}000$), the oil and water were always in the dispersed flow

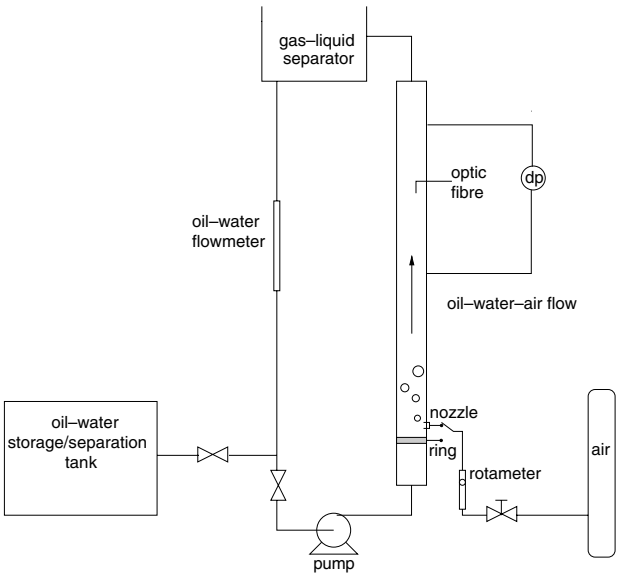


Fig. 2. Sketch of the three-phase loop.

regime due to turbulent mixing. The fluids used are air, tap water and Shell Macron oil. A summary of the data for the experiments at the Kramers Laboratorium and the Donau loop are listed in Table 1.

### 2.2. Measurement techniques

A differential pressure transducer is placed in the test section part of the loop, with $\Delta h = 2$ m between the two points. The pressure measurements are accurate with a relative error of 0.5%. Volumetric flow rate and mixture density are given by a Coriolis flow meter placed in the downcoming part of the loop, where only liquids flow. Assuming a homogeneous mixture of the oil and the water, the water fraction can be deduced by linear interpolation: $\epsilon = (\rho_{\text{mix}} - \rho_{\text{oil}})/(\rho_{\text{water}} - \rho_{\text{oil}})$. For each run, after waiting long enough for stable flow to be established, these variables are recorded for at least one minute at a sampling frequency of 1 Hz. The experiments are performed at temperatures of the liquids between 18 °C and 25 °C, so the viscosity change is not significant. The effective mixture viscosity of the oil–water was measured in a Couette flow rheometer (Contraves Rheomat 115), for oil dispersed in water. The oil–water mixture was emulsified using Triton X-100 as a surfactant. For the oil–water pipe flow the in-line oil–water mixture viscosity can be different because of the difference in drop size and the absence of surfactant.

For local measurements optical fibre probes have been widely used and validated for detecting bubbles in pipes or columns (Julia et al., 2005). The technique is mainly used for air bubbles in water, however it functions also in the presence of oil, though with less accuracy. The principle relies on the difference in refractive index of the probe and the surrounding media. Light is emitted at one end of the fibre probe and conducted to the probe tip. Depending on which phase surrounds the probe tip, light is partly reflected. The reflected intensity is measured and converted to a voltage. The local time-averaged void fraction can be derived, as well as bubble size and velocity when a second tip is used. In theory the probe can discriminate between oil, air and water, since the refractive index is different for the different combinations (see Table 2).

Table 2
Refractive index of the probe and fluids

| Media | Refractive index |
|---|---|
| Silica | 1.459 |
| Air | 1.0 |
| Water | 1.33 |
| Oil | 1.445 |

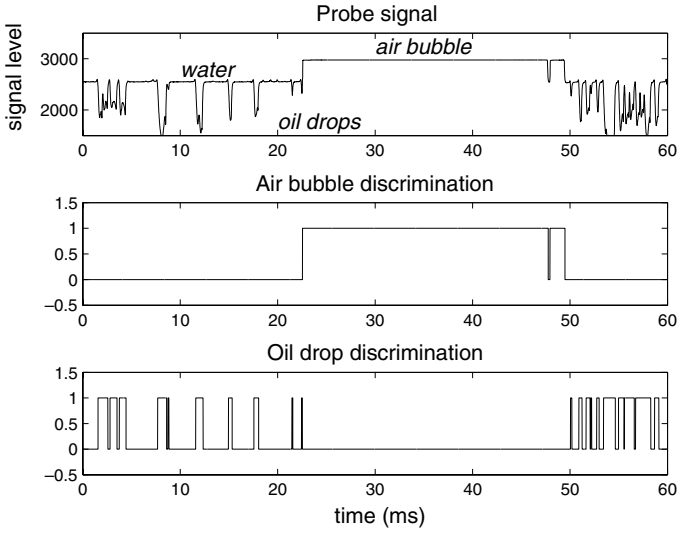


Fig. 3. Probe detection and data processing for air bubbles in oil-in-water flow.

In practice, there are two difficulties associated with the presence of oil: (i) the difference in refractive index between the fibre tip and the oil is small and (ii) the oil might stick to the tip depending on the wettability of the fibre. However, by performing a careful data processing these effects can be minimized. An algorithm developed by Wouter Harteveld (Harteveld, 2005) was used and adapted for the present experiments. An example of the bubble/drop detection procedure is shown in Fig. 3 for oil drops and air bubbles in water.

The calculation of the time-averaged void fraction has been validated and proved to be accurate (Guet, 2004 and Harteveld, 2005) within less than 5%, for gas–liquid flow. Concerning bubble size and velocity some comparisons have been made between optical fibre probe measurements and high speed video recordings. After processing the value given by the probe exhibits an uncertainty range of 15%, which is relatively high. However, during the experiments the bubble size varies from 1 mm to more than 20 mm, so it is still relevant to make use of the size and velocity data for such a range of conditions.

## 3. Two-phase oil–water flow

In order to characterize the behaviour of oil–water flow as the water fraction (or water cut, which is the fraction of water present in the liquid phase) reaches the phase inversion point, oil–water experiments were first conducted. Water fractions ranging from 100% to 30% were investigated. For this range of water fractions the dispersion is an oil-in-water dispersion. After each oil concentration that we studied the liquids were separated, the concentration was changed and the liquids were mixed again. (This type of experiment is called a *direct route experiment*.) In Fig. 4, the pressure gradient measured for an oil–water flow is presented as a function of the liquid mixture velocity for different values of the water fraction. As can be seen the pressure drop decreases with decreasing water fraction up to a value of 36%; thereafter the pressure drop increases with decreasing water fraction due to the inversion process. To ensure that the oil is finely dispersed in the water, only mixture velocities above 0.9 m/s were considered.

The total pressure gradient can be written as the sum of the gravitational component $\rho_m g$, where $\rho_m$ is the mixture density, and a frictional component $\rho_m f_m U^2/2D$ in which $f_m$ is the friction factor. In vertical pipe flow the total pressure gradient is dominated by the gravitational part, but as the mixture velocity increases the frictional component of the pressure gradient becomes more important. In Fig. 4 also the pressure gradient for water alone is given as obtained from well-known friction factor correlations for turbulent flow. As can be seen the Blasius correlation for a pipe with a smooth wall

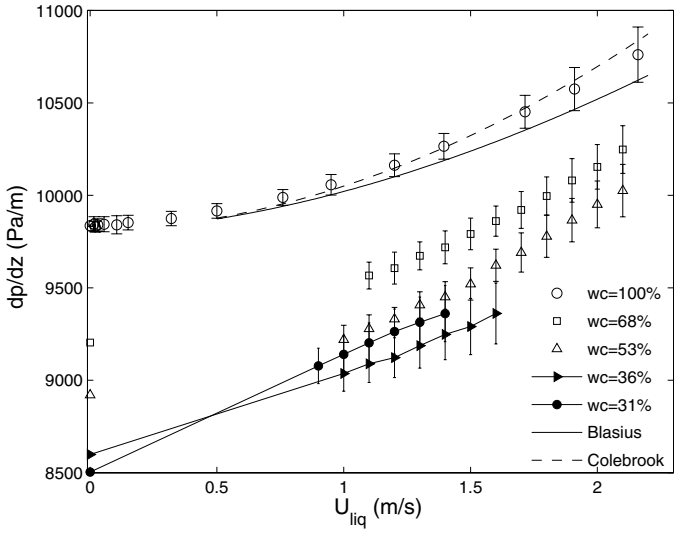


Fig. 4. Pressure gradient as function of mixture velocity for oil–water flows at different water fractions. Closed symbols corresponds to experiments close to phase inversion. The water fraction is indicated by wc (water cut).

$$f_m = 0.316/Re^{0.25} \tag{1}$$

slightly underpredicts the pressure gradient. A better agreement is found with the Colebrook equation

$$\frac{1}{\sqrt{f_m}} = -2\log\left(\frac{\varepsilon/D}{3.71} + \frac{2.52}{Re\sqrt{(f_m)}}\right), \tag{2}$$

where $\varepsilon$ is the pipe roughness, with $\varepsilon = 10^{-5}$ m in Fig. 4. For viscosity calculation, the use of an explicit expression for the friction factor, such as in Eq. (1), is more convenient. The following interpretation can now be given for results shown in Fig. 4. At high values of the water fraction the pressure gradient decreases with decreasing water fraction because of the reduced mixture density (as oil is lighter than water). However with decreasing water fraction also the friction factor of the oil–water mixture grows. Therefore at a sufficiently low value of the water fraction of 36% (close to the point of phase inversion around a water fraction of 30%) and for sufficiently large mixture velocities, the pressure gradient starts to increase again with decreasing water fraction. This is in particular due to the sharp increase of the mixture viscosity at phase inversion. Assuming that the friction factor follows the Blasius expression and using the measured value of the pressure gradients, the mixture viscosity can be estimated. The result is given in Fig. 5.

For dense liquid–liquid dispersion several other empirical relations are available for calculating the effective mixture viscosity (Brauner, 1998) based on the fraction of the dispersed phase. In Fig. 5 the relation derived by Krieger and Dougherty (1959) is plotted

$$\mu_m = \mu_w\left(1 - \frac{\phi}{\phi_c}\right)^{-2.5\phi_c}, \tag{3}$$

where $\mu_w$ is the water viscosity, $\phi$ the water fraction and $\phi_c$ the maximum packing concentration (assumed to be 0.74 in this figure). Also viscosity measurements performed with a Couette flow rheometer are shown. It appears that the mixture viscosity estimated from the Blasius correlation for turbulent flow is consistent with the rheometer measurements and the Krieger–Dougherty relation down to a water fraction of 40%. For a water fraction close to phase inversion (around 30%) there is a large spread in the measurement results for the mixture viscosity obtained at different mixture velocities. This might be due to the occurrence of laminar flow, which is supported by the observation of the linear variation of the pressure gradient with respect to velocity for a water fraction of 31% and 36% (closed symbols on Fig. 4). Mixture viscosities obtained from the single-phase laminar friction factor $f_m = 64/Re$ lead to a somewhat better agreement with the Krieger–Dougherty relation. However, the main point we want to make is, that Fig. 5 emphasizes the dramatic increase

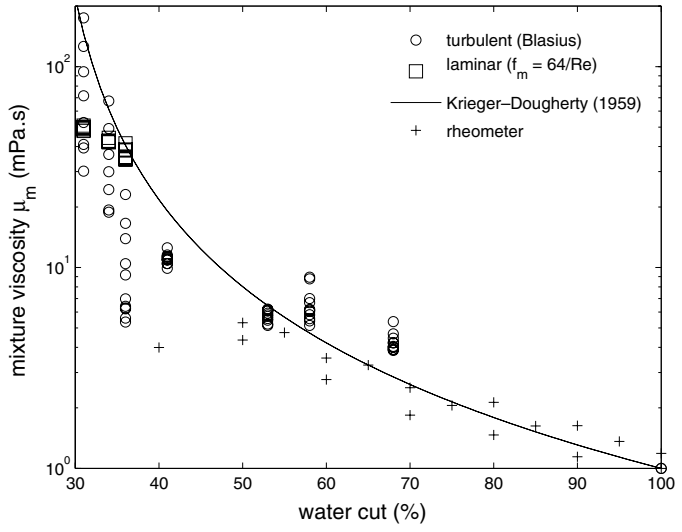


Fig. 5. Oil–water flow: mixture viscosity directly measured (rheometer) and calculated from measurements.

in oil–water mixture viscosity around phase inversion. This is perhaps due to a non-Newtonian behaviour (as mentioned by Pal (1990)) of the mixture at the point of phase inversion.

## 4. Three-phase oil–water–air flow: influence of the gas injector

### 4.1. Procedure

In the following water fractions ranging from 100% to 10% have been investigated. After introducing the desired concentration of oil in the pipe the pump was started in order to have a constant liquid mixture velocity, and gas was injected at a constant superficial velocity of approximately 0.06 m/s for all experiments. Total liquid velocities of 1 m/s and 1.5 m/s have been applied. At these velocities the flow regime is dispersed and the frictional contribution to the pressure drop is not negligible. After reaching steady state measurements were carried out including detailed optical fibre probe measurements at six different positions in the radial direction of the pipe. A switch connection allowed us to choose either the nozzle injector for injecting large bubbles or the ring injector for smaller bubbles.

### 4.2. Flow patterns

In Fig. 6, the difference in flow patterns caused by the change of injector is clear: the ring injector produces small bubbles of a rather constant size and with an ellipsoidal shape, whereas the nozzle injector produces a wide range of bubble sizes from very small spherical bubbles (around 1 mm) to large Taylor bubbles (several pipe diameters in chord length).

Theses pictures are for pure water. When oil is present in the pipe, it becomes difficult to observe individual bubbles because the oil–water mixture tends to be opaque due to the very small drops of the dispersed phase. Information about the local void fraction is provided by the optical fibre probe (Fig. 7). As described in a study by Guet (2004) small bubbles move towards the wall, whereas large bubbles remain in the centre of the pipe. Therefore the ring injector generates a "wall-peaking" profile for the gas fraction and the nozzle injector a "core-peaking" profile.

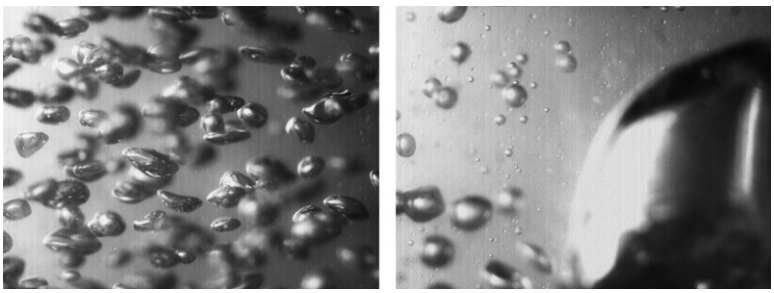

Fig. 6. Air–water flow: example image of bubbles generated by the ring (left) and the left (right) injector (image width ≈35 mm).

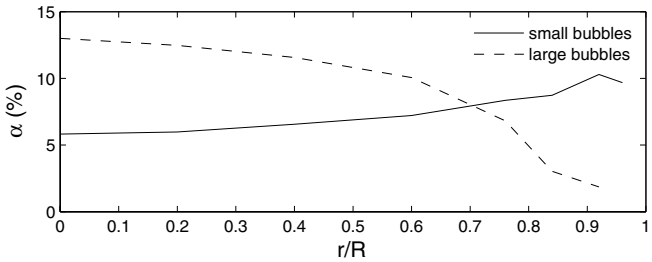


Fig. 7. Air–water flow: local gas void fraction $\alpha$ for the two types of injector at $U_{water} = 0.54$ m/s and $U_{air} = 0.03$ m/s.

### 4.3. Pressure measurements

In Fig. 8 the pressure gradient is plotted as a function of water fraction for the air–water–oil case and for the water–oil case. As can be seen phase inversion occurs at a water fraction of around 30% within a range of ±5%.

The pressure gradient is higher for water–oil flow than for the air–water–oil flow. However, this difference disappears close to phase inversion. Also the pressure gradient is generally smaller for smaller injected bubbles (ring injector), when compared with large injected bubbles (nozzle injector). Around the point of phase inversion the pressure fluctuations become stronger. This increases the uncertainty range in the experimental results; within the larger error bars the two types of injector give about the same pressure gradient in this region. In accordance with the experiments of Descamps et al. (2006) the pressure gradient is significantly larger at the point of phase inversion. Outside the phase inversion region the influence of the gas injection type on the pressure gradient is more clearly visible when oil is the continuous phase than for water as the continuous phase: injecting small bubbles (with the ring injector) significantly reduces the pressure gradient. It will be shown in Section 4.5 that the change in bubble size with oil concentration may explain this result.

### 4.4. Local concentration

In Fig. 9 the local gas void fraction is plotted as function of the normalized distance to the pipe wall for different values of the water fraction for the case of an oil-in-water mixture (water is the continuous phase and oil the dispersed one).

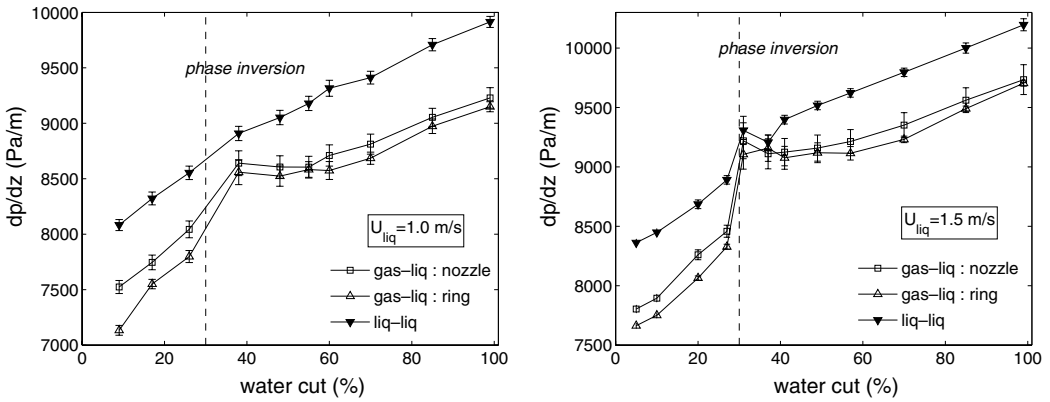


Fig. 8. Pressure gradient for water–oil flow and air–water–oil flow.

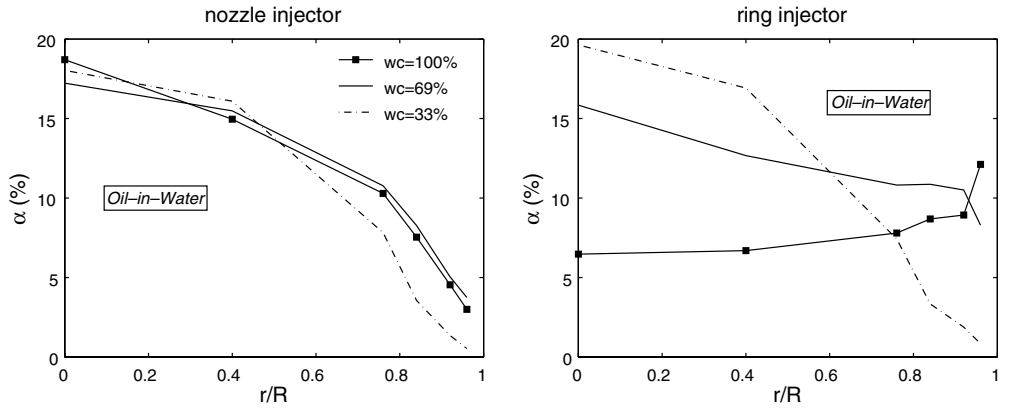


Fig. 9. Local gas void fraction for the two types of injector in an oil-in-water flow, at $U_{sl} = 1$ m/s and $U_{sg} = 0.06$ m/s.

It can be seen that for this range of water fractions the gas profile for the nozzle injector remains approximately the same: a "core-peaking" profile. As the oil concentration increases, even more gas is located in the core and less at the wall. So the core-peaking profile is more pronounced. Regarding the ring injector the initial profile is "wall-peaking" but as the oil concentration increases there is a transition to a core-peaking profile (at approximately 70% of water fraction).

After phase inversion (at a water fraction of 30%) there is a water-in-oil flow and the value of the void fraction seems to drop slightly for both gas injectors, as shown in Fig. 10.

Since the superficial velocity of air remains the same, this decrease in void fraction is probably due to a change in bubble size, and associated with that, a change in the bubble–liquid slip velocity. Moreover, after phase inversion the gas void fraction profile for the ring injector is not core-peaking anymore. It looks more like the initial wall-peaking profile (Fig. 10, right). So it seems that for this injector, starting with pure water and gradually increasing the oil concentration, a first transition between a wall-peaking profile and a core-peaking profile takes place around a value of 70% of the water fraction. The void fraction profile then tends to follow a similar behaviour as for the nozzle injector with more air present in the core as the oil concentration continues to increase. At phase inversion a second transition occurs, but in the reverse way: the core-peaking profile switches to a wall-peaking profile.

### 4.5. Bubble size and velocity

#### 4.5.1. Air–water flow

The types of bubbles generated by the nozzle and ring injectors are shown in Fig. 11, where the bubble chord length and velocity are plotted for a sample of bubbles measured in the middle of the pipe, for a bulk velocity of the liquid of 1 m/s.

Larger bubbles rise faster than smaller ones but have also a larger drag. This can be seen by the derivative of the velocity with respect to the chord length: for large bubbles (chord length above 10 mm) the derivative is lower than for smaller bubbles. This can be associated to the shape of the bubbles, which is not spherical anymore above a critical size. Unfortunately it is not possible with the two-point probe to get information on the shape of the bubbles. It is important to point out, that the nozzle injector also produces small bubbles, as shown qualitatively in Fig. 6. Fig. 12 validates this fact quantitatively for air–water flows.

In this figure the bubble size distribution for the nozzle injector is bimodal with one mode around 3 mm and another mode at 20 mm. The bubble size distribution for the ring injector is "included" in the first mode. This means that the nozzle injector produces large Taylor bubbles as well as small spherical bubbles, usually entrained in the wake of the large bubbles. When looking at the same distributions close to the wall (Fig. 12, right), the second mode of the nozzle injector distribution has disappeared, which is expected since large bubbles are not present close to the wall. For the sake of simplicity, the arithmetic mean has been chosen to average the bubble size in the following.

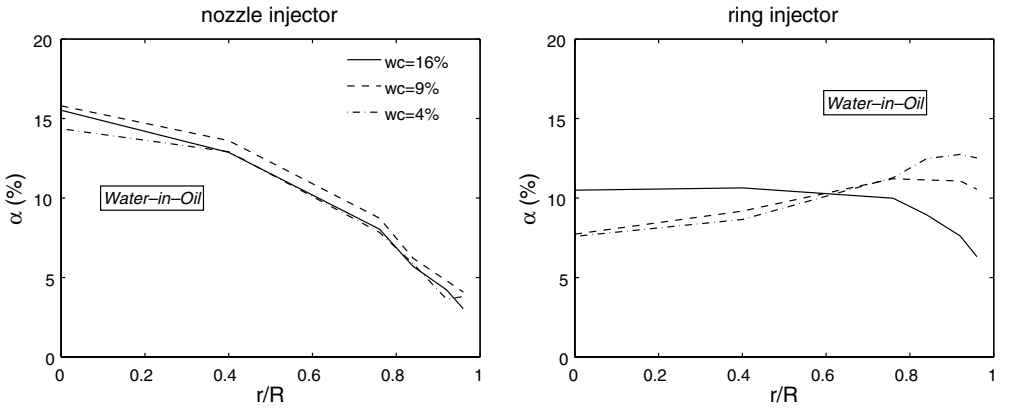


Fig. 10. Local gas void fraction for the two types of injector in water-in-oil flow, at $U_{sl} = 1$ m/s and $U_{sg} = 0.06$ m/s.

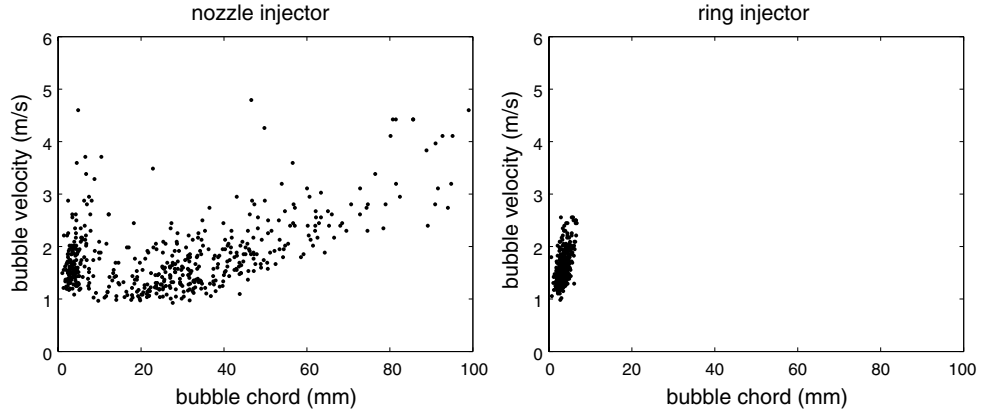


Fig. 11. Bubble chord and length for air–water flow, measured in the centre of the pipe.

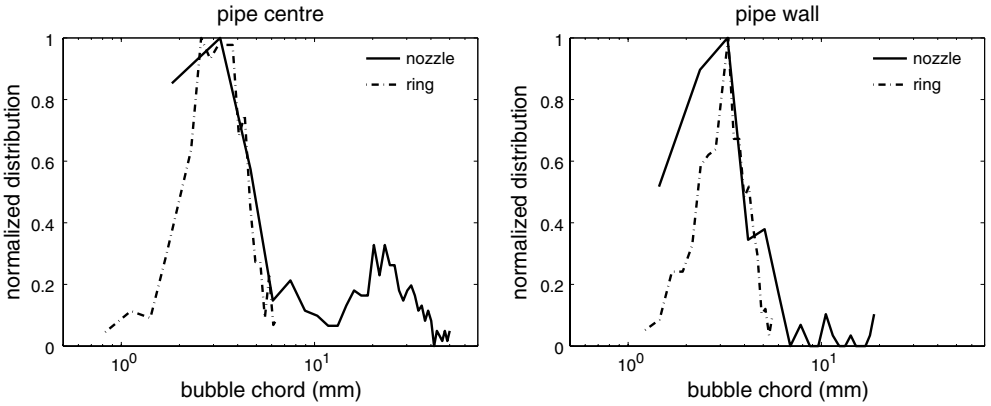


Fig. 12. Bubble size distribution for an air–water flow.

*4.5.2. Oil–water–air flow*

For both injectors, the bubble size increases with increasing oil concentration up to phase inversion (Fig. 13).

The tendency is more dramatic for the small bubbles generated by the ring injector, as shown in Fig. 13. For pure water the size of the bubbles from the ring injector is around 4 mm at the pipe centre as well as close to the wall. At the pipe centre when the water fraction is decreased from 100% down to 70%, the bubble size increases slightly. However for a water fraction decreasing from 70% to 30% (still oil-in-water dispersion) the bubble size in the pipe centre increases sharply to almost the bubble size generated by the nozzle injector. This critical water fraction of 70% at which the bubbles start to grow corresponds to the transition from wall-peaking to core-peaking for the ring injector mentioned previously. Below the phase inversion (water-in-oil conditions) the bubble size in the pipe centre reduces considerably for both injectors. It is worth noticing that for both injectors the bubbles are smaller for water-in-oil conditions than for oil-in-water conditions. A similar behaviour for bubbles close to the pipe wall is observed as described above for bubbles at the pipe centre, but the increase in bubble size is less visible since large bubbles tend to migrate out of this region.

In Fig. 14 the bubble velocity is shown as function of the water fraction for the two types of injectors.

For values of the water fraction between 70% and 100% the velocities for bubbles generated by the ring injector are smaller than those generated by the nozzle injector. The reason is that in the region of water fractions the ring injector bubbles are smaller than the nozzle injector bubbles. However, for lower values of the water fraction (between 70% and the point of phase inversion) there is no significant difference in velocity

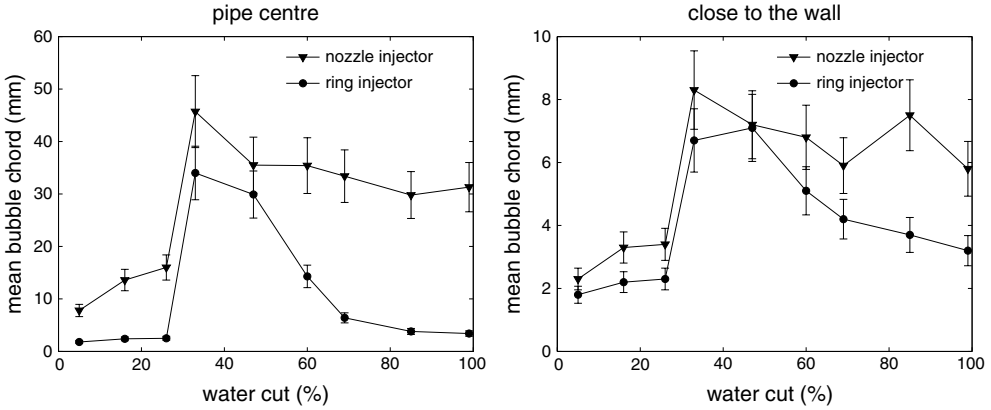


Fig. 13. Mean bubble size for oil–water–air flow, at $U_{sl} = 1$ m/s and $U_{sg} = 0.06$.

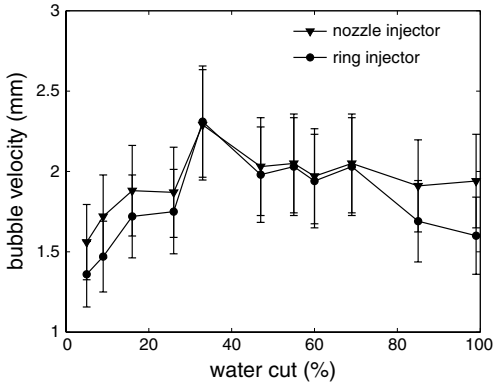


Fig. 14. Oil–water–air flow: evolution of mean bubble velocity as a function of water cut at the pipe centre, at $U_{sl} = 1$ m/s and $U_{sg} = 0.06$.

between the bubbles generated by both injectors. After phase inversion the bubble velocity decreases for both injectors, because (as mentioned in Section 4.5) the bubble size reduces when oil is the continuous phase.

### 4.6. Discussion

An important conclusion of our investigation is, that oil drops cause an increase in the size of air bubbles present in a continuous water phase. This is not the case for water drops present in a continuous oil phase. This effect is in particular dramatic for the ring injector, as the initial bubbles are small. This can easily be observed visually by taking pictures, as shown in Fig. 15. The bubbles are of the size of 1 cm in the oil-in-water case (Fig. 15 top) whereas in the water-in-oil case the bubbles are closer to millimeter dimensions (Fig. 15 bottom).

Therefore when small air bubbles are injected by the ring injector, a wall-peaking profile of the gas phase is only found at low concentrations of the oil drops. At higher values of the oil drop concentration the air bubbles grow in size, move to the pipe centre and cause a core-peaking profile. With a further increase in oil drop concentration the bubbles continue to grow and become largest at the point of phase inversion. Thus it is no surprise that the pressure gradient results obtained for the two type of injectors are close to each other around the point of phase inversion. After phase inversion when oil is the continuous phase, the bubbles become small again over the complete region of values of oil concentration between the point of phase inversion and 100%

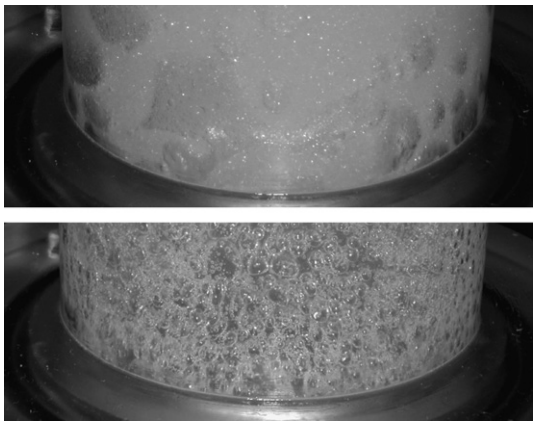

Fig. 15. Picture of the ring gas injection for oil-in-water (top) and water-in-oil (bottom) (width of the pipe = 50 mm).

oil. Hence, in this case the effect of introducing small bubbles in the water-in-oil flow is again beneficial in terms of gas-lift, as it reduces the pressure gradient when compared to larger bubbles (Fig. 8).

The maximum stable size that a bubble can achieve is the result of a balance between coalescence and break-up. Coalescence is more efficient at lower turbulence intensity and break-up increases at higher turbulence intensity. It is well known that the viscosity of an emulsion increases exponentially with increasing volume fraction of the dispersed phase (Brauner, 1998 and Fig. 5). This explains perhaps why the bubble size increases in the oil-in-water dispersion: with increasing concentration of oil drops (up to 70% of the liquid phase) the effective viscosity becomes higher and the turbulence will be more suppressed. As a result the balance between bubble break-up and bubble coalescence shifts towards bubble coalescence and larger bubbles are formed. According to this reasoning the bubbles should then decrease in size when with decreasing water fraction phase inversion occurs and oil becomes the continuous phase. The fraction of the dispersed phase (water) after phase inversion is much less (less than 30%) than the dispersed phase fraction (about 70% of oil drops) before inversion. As a result the mixture viscosity of the water-in-oil dispersion is lower than the mixture viscosity of the highly concentrated oil-in-water dispersion. Furthermore, the oil–air surface tension is lower than the water–air surface tension, which also favours the occurrence of smaller bubbles. This is confirmed by our experiments: the bubbles are significantly smaller when oil is the continuous phase than when water is the continuous phase. However this interpretation needs to be validated by oil–water viscosity measurements over the complete range of water fractions.

## 5. Three-phase oil–water–air flow: influence of the gas and liquid superficial velocity

The influence of the gas and liquid superficial velocity on the three-phase oil–water–air flow was studied in detail. Only one gas injector (large bubble nozzle injector) was used. The reason is, that it produces a core-peaking gas fraction profile which can be measured more accurately. The water fraction varied from 100% to 30% (oil-in-water dispersion), and the gas and liquid mixture superficial velocities were changed.

### *5.1. Pressure measurements*

At constant gas flow rate and increasing liquid mixture velocity (Fig. 16a) the pressure gradient increases because of a higher friction.

For a water fraction around 30%, close to phase inversion, the increase is even more pronounced because of the significantly larger oil–water effective viscosity (Section 3). At constant liquid mixture velocity and increasing gas superficial velocity (Fig. 16b), the pressure gradient is reduced, due to the lower gravitational pressure drop over the pipe when more gas is present. However, it appears that close to phase inversion, this gravitational effect tends to vanish. This can also be seen in Fig. 17, where the gas–liquid normalized pressure

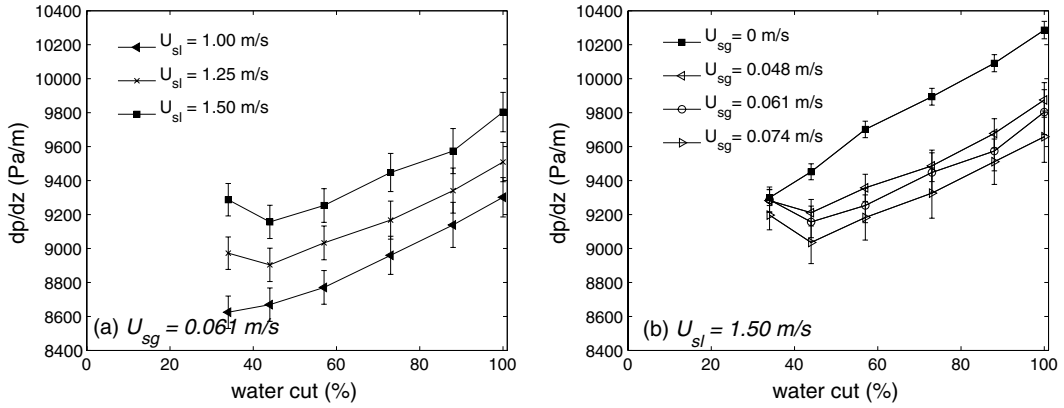


Fig. 16. Oil–water–air pressure gradient for oil-in-water dispersion: (a) effect of the liquid superficial velocity at constant gas superficial velocity, (b) effect of the gas superficial velocity at constant liquid superficial velocity.

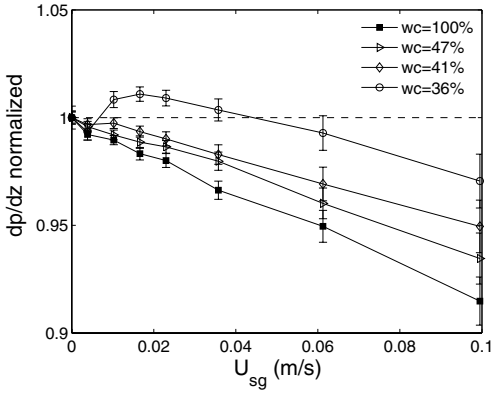


Fig. 17. Oil–water–air pressure drop normalized by the oil–water pressure drop, at $U_{\text{liquid}} = 1.5$ m/s.

gradient (which is the ratio of the gas–liquid mixture pressure drop to the liquid mixture pressure drop) is presented as a function of the gas superficial velocity, for different water cuts.

For most conditions injecting gas results in a lower pressure gradient (normalized pressure drop is smaller than 1). However, for a water cut of 36%, there exist a range of gas flow rates for which the gas–liquid mixture pressure gradient is higher than the liquid mixture pressure gradient (normalized pressure drop is higher than 1). This suggests that the presence of gas in the pipe dramatically increases the frictional component of the pressure gradient, which is usually not dominant in vertical flow. The total gas liquid pressure gradient can be decomposed as follows:

$$\frac{\mathrm{d}p}{\mathrm{d}z} = (1-\bar{\alpha})\rho_{\text{mix}}g + F_{\text{l}} + F_{\text{gl}}, \tag{4}$$

where $\bar{\alpha}$ is the total gas fraction over the cross-section, which is integrated from the local radial gas fraction, $\rho_{\text{mix}}$ is the oil–water mixture density, $F_{\text{l}}$ is frictional pressure gradient of the liquid mixture (independent of the bubbles), and $F_{\text{gl}}$ is the gas–liquid frictional pressure gradient (due to the bubble agitation). The total friction component can be explicitly expressed in air–water flow, using various correlations, such as the correlation of Lockhart and Martinelli (1949). In Fig. 18 the evolution of $\bar{\alpha}\rho_{\text{mix}}g$ and $F_{\text{gl}}$ is plotted against the gas superficial velocity for pure water (a) and close to phase inversion (b). (Note that in this figure the term $\bar{\alpha}\rho_{\text{mix}}g$ has to be taken as a negative contribution to the pressure balance).

The gas gravitational term $\bar{\alpha}\rho_{\text{mix}}g$ is always greater than the frictional term $F_{\text{gl}}$ for pure water (Fig. 18a), which means that the total pressure drop of air–water flow is lower than the single-phase water pressure drop.

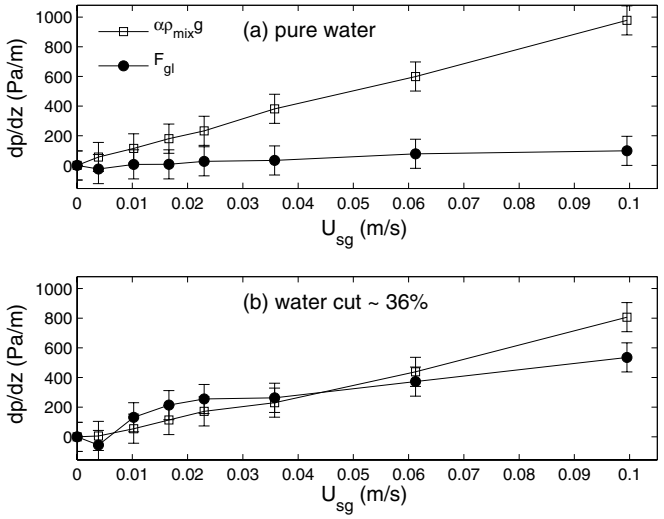


Fig. 18. Gas gravitational term ($\bar{\alpha}\rho_{\text{mix}}g$) and frictional term ($F_{\text{gl}}$) of the total pressure gradient, at $U_{\text{liquid}} = 1.5$ m/s: (a) air–water flow, (b) oil–water–air flow around oil–water phase inversion.

When the water cut is close to phase inversion (Fig. 18b), the balance between the gravitational term and the frictional term is more equally distributed, which makes it possible for the friction to overcome the gravity term. For the purpose of gas-lifting in oil production this means a counter productive effect for this range of conditions. It can be assumed that the local distribution of oil, water and air may have some influence on the pressure gradient variations as the mixture close to the wall will determine the friction part of the pressure gradient.

### 5.2. Local concentration

The large bubble nozzle injector generates a core-peaking gas fraction profile, as shown on Fig. 19. This figure corresponds to the same case as that of Fig. 17. There is no significant difference whether the liquid phase is pure water (Fig. 19 left) or an oil-in-water mixture close to phase inversion (Fig. 19 right). For a low gas superficial velocity ($U_{\text{sg}} = 0.004$ m/s) the void fraction is more concentrated in the core of the pipe when the liquid phase is close to phase inversion than when the liquid phase is pure water.

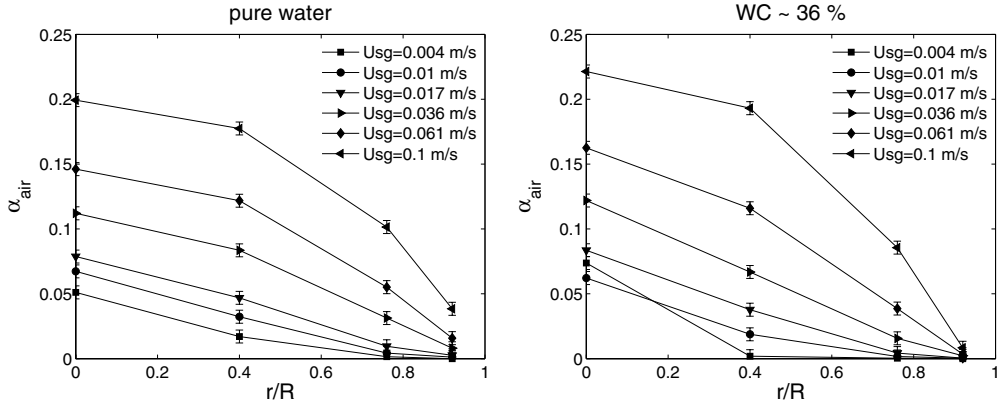


Fig. 19. Gas void fraction profile for different gas superficial velocity, at $U_{\text{liquid}} = 1.5$ m/s.

In Fig. 20 the local concentration of water and oil is plotted against gas superficial velocity, for a water cut close to phase inversion (same case as that represented on Fig. 19 right). Three radial positions are shown: one corresponding to the centre of the pipe ($r/R = 0$), and two corresponding to the wall region ($r/R = 0.76$ and $r/R = 0.92$). Because of a weaker oil signal given by the probe (see Fig. 3), the signal analysis leads to a relatively large uncertainty range, of the order of $\pm 10\%$. Thus only qualitative appreciation is relevant, however some trends can be identified. First, the water and oil phases are not homogeneously distributed over the cross-section: water tends to accumulate at the wall (the concentration for $r/R = 0$ is smaller than the concentration for $r/R = 0.92$), whereas oil tends to stay in the core pipe region (the concentration for $r/R = 0$ is higher than the concentration for $r/R = 0.92$). Second, as the air superficial velocity is increased, the core of the pipe is more occupied by the gas, and as a result the oil and water distribution becomes more homogeneous, which is shown on Fig. 20 by the convergence of the radial fraction towards a more narrow range of values. In other words, as the gas flow rates increases, for a constant water fraction, the oil that was originally in the core of the pipe is pushed towards the wall.

### 5.3. Discussion

With respect to the influence of gas and liquid superficial velocity, the singular balance between friction and gravity close to phase inversion is highlighted here. At increasing liquid superficial velocity and constant gas flow rate, the frictional pressure gradient becomes more significant and, as a result, the total pressure gradient increases. This effect becomes stronger as the water fraction is decreased since the liquid mixture is then more viscous, as shown on Fig. 5.

When gas superficial velocity is increased for a constant liquid flow rate, the gravitational term of the pressure gradient is increased. However it appears that the frictional component may increase in the same extent, and even overcome the gravity term, leading to a higher pressure gradient, although more gas is present. Hence there is an extra friction term due to the presence of the air. One explanation could be found in the local phase distribution. Indeed, for the case studied the oil concentration profile in the absence of bubbles seems to be: core-peaking. As more and more bubbles are introduced, the oil tends to spread towards the wall because the bubbles occupy the core, which may induce a higher wall friction because the oil viscosity is higher than the water viscosity. However this interpretation should be confirmed by experimental data closer to the wall, in order to capture the viscous sub-layer. Furthermore, the profile of the oil concentration may not always be core-peaking depending on the liquid mixture velocity and water cuts. It was shown in a recent work

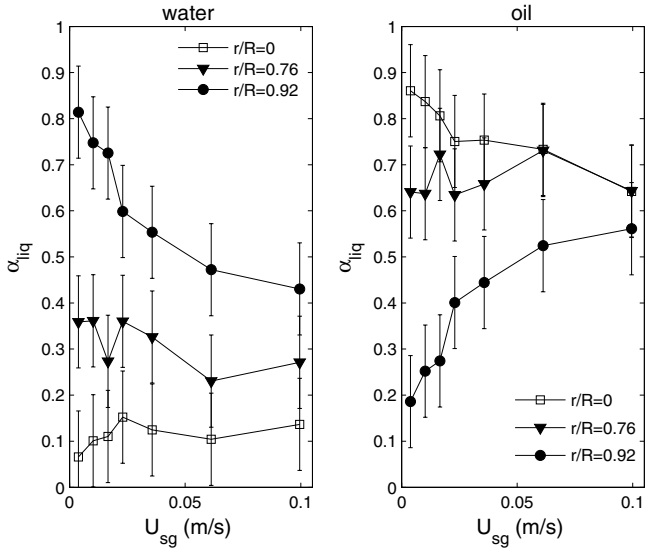


Fig. 20. Oil–water–air flow: local concentration of water and oil at different radial positions, at water cut = 36% and $U_{\text{liquid}} = 1.5$ m/s.

(Zhao et al., 2006) on oil–water vertical flow that the oil concentration profile can evolve from a core-peaking profile to a wall-peaking profile when changing the input water and oil flow rates. Also it should be noted that the flow patterns were studied in a Perspex pipe, which is hydrophobic, so an oil film is expected to be present at the wall.

The extra friction term when air is present might also be explained by the action of the bubbles on the flow. Although the gas follows a core-peaking fraction profile, some gas is still present in the wall region. Studies on air–water flow have underlined the action of bubbles on the turbulence. For instance, Sato et al. (1981) decomposed the total shear stress into a mean part, a liquid turbulent part, and a bubble induced turbulent part. This process could play a role here, and in combination with the increased oil–water viscosity around phase inversion, lead to a frictional term that cancels the effect of the gravity term. Moreover, it is reasonable to assume that small bubbles travel close to the wall, and may periodically ''bounce'' on the viscous sub-layer. One could then consider the flow close to the wall to be a steady current superimposed by an oscillatory motion. In this case, it is known that the mean wall shear stress can increase or decrease depending on the flow regime (Lodahl et al., 1998). In the case of an increase, the frictional pressure gradient will be increased as well.

## 6. Conclusions

Three-phase (oil–water–air) flow has been studied experimentally in order to better understand earlier results by Descamps et al. (2006) for the gas-lift technique applied to oil–water flows. Particular attention was paid to the question, whether the advantage of using small bubbles as found for water–air flows also holds for oil–water–air flows. To that purpose air bubbles were injected by means of two different injectors: a nozzle injector, for large bubbles, and a ring injector, for smaller bubbles. It was shown that when water was the continuous phase (in practice water is usually the continuous phase during the later stages of production), the bubble size increases with increasing oil concentration. Close to phase inversion the bubble size was even similar for the two types of injector, thus the beneficial effect of injecting small bubbles was limited. When oil was the continuous phase, the bubbles injected by the ring injector remained small and improved the efficiency of the gas-lift technique. Hence the break-up and coalescence mechanisms determining the size of the bubbles, seem to play different roles depending on which phase is the continuous one.

Finally it was shown, that the pressure gradient close to phase inversion can even increase by gas injection. This confirms the results presented in Descamps et al. (2006). Under such conditions the gas-lift technique would become counter-productive for oil recovery. The combination of a high oil–water effective viscosity and a complex balance between the frictional and gravitational pressure gradients may explain this phenomenon.

## Acknowledgements

The authors acknowledge the financial support given by FOM (Foundation of Fundamental Physics in The Netherlands).

## References

Brauner, N., 1998. Liquid–liquid two-phase flow. HEDU – Heat Exchanger Design Update, 1–40, chapter 2.3.5.

Brauner, N., Ullmann, A., 2002. Modeling of phase inversion phenomenon in two-phase pipe flows. Int. J. Multiphase Flow 28, 1177–1204.

Chesters, A.K., Issa, R., 2004. A framework for the modelling of phase inversion in liquid–liquid systems. In: 5th International Conference on Multiphase Flow, ICMF'04, Yokohama, Japan.

Descamps, M., Oliemans, R.V.A., Ooms, G., Mudde, R.F., Kusters, R., 2006. Influence of gas injection on phase inversion in an oil–water flow through a vertical tube. Int. J. Multiphase Flow 32, 311–322.

Guet, S., 2004. Bubble size effect on the gas-lift technique. Ph.D. thesis, Delft University of Technology.

Guet, S., Ooms, G., Oliemans, R.V.A., Mudde, R.F., 2003. Bubble injector effect on the gaslift efficiency. AIChE J. 49, 2242–2252.

Harteveld, W., 2005. Bubble columns: structures or stability? Ph.D. thesis, Delft University of Technology.

Ioannou, K., Nydal, O.J., Angeli, P., 2005. Phase inversion in dispersed liquid–liquid flows. Exp. Therm Fluid Sci. 29, 331–339.

Julia, J.E., Harteveld, W.K., Mudde, R.F., Van den Akker, H.E.A., 2005. On the accuracy of the void fraction measurements using optical probes in bubbly flows. Rev. Sci. Instrum. 76, 035103.

Krieger, I.M., Dougherty, T.J., 1959. A mechanism for non-newtonian flow in suspensions of rigid spheres. Trans. Soc. Rheology 3, 137–152.

Lockhart, R.W., Martinelli, R.C., 1949. Proposed correlation of data for isothermal two-phase two-component flow in pipes. Chem. Eng. Prog. 45, 39–48.

Lodahl, C.R., Sumer, B.M., Fredsøe, J., 1998. Turbulent combined oscillatory flow and current in a pipe. J. Fluid Mech. 373, 313–348.

Pal, R., 1990. On the flow characteristics of highly concentrated oil-in-water emulsions. Chem. Eng. J. 43, 53–57.

Piela, K., Delfos, R., Ooms, G., Westerweel, J., Oliemans, R.V.A., Mudde, R.F., 2006. Experimental investigation of phase inversion in an oil–water flow through a horizontal pipe loop. Int. J. Multiphase Flow 32, 1087–1099.

Sato, Y., Sadatomi, M., Sekoguchi, K., 1981. Momentum and heat transfer in two-phase bubble flow – I. Theory. Int. J. Multiphase Flow 7, 167–177.

Zhao, D., Guo, L., Hu, X., Zhang, X., Wang, X., 2006. Experimental study on local characteristics of oil–water dispersed flow in a vertical pipe. Int. J. Multiphase Flow 32, 1254–1268.